Density of states determined from Monte Carlo simulations

J. Hove*
Bergen Centre for Computational Science, 5020 Bergen, Norway
(Received 24 January 2004; revised manuscript received 14 June 2004; published 19 November 2004)

We describe a method for calculating the density of states by combining several canonical Monte Carlo runs. We discuss how critical properties reveal themselves in $g(\epsilon)$ and demonstrate this by applying the method to several different phase transitions. We also demonstrate how this can used to calculate the conformal charge, where the dominating numerical method has traditionally been the transfer matrix.

DOI: 10.1103/PhysRevE.70.056707 PACS number(s): 05.10.Ln, 05.50.+q, 64.10.+h, 75.40.Mg

I. INTRODUCTION

Since it was devised by Metropolis *et al.* in 1953 [1], Monte Carlo (MC) simulations based on the Metropolis algorithm have had a tremendous impact on physics; SIAM recently rated the algorithm among the ten most influential numerical algorithms of the previous century [2]. For a historical summary and a review of modern MC methods, we refer to the proceedings of the conference hosted to celebrate the 50th anniversary of the algorithm [3]. For general references to Monte Carlo simulations see, e.g., Refs. [4–6].

The Metropolis algorithm is well suited to calculate quantities which can be expressed as

$$\langle O\rangle = \frac{1}{N}\sum_i \hat{O}|\psi_i\rangle, \tag{1}$$

i.e., as averages of values obtained by operating an operator $\hat{O}$ on a series of states $|\psi_i\rangle$. Focusing on phase space Eq. (1) can be denoted a *local* estimator, in the sense that only one point in phase space is involved at a time. Some quantities like entropy and free energy cannot be expressed like Eq. (1); their evaluation requires simultaneous knowledge of global portions of phase space. Entropy and free energy can in principle be obtained by thermodynamic integration [4,5],

$$F(T) = U(T) - T\int_0^T \mathrm{d}T' \frac{C_V(T')}{T'}, \tag{2}$$

but this technique does not seem to be used much.

Equation (1) represents the absolutely simplest way to get MC results. A simulation produces a series of states $|\psi_i\rangle$ distributed according to the Boltzmann distribution; the mean over these states is calculated. Both the initial step of obtaining the data and the final post-processing can be done differently. With multicanonical sampling [7–9] the Markov chain is altered to (ideally) yield a *flat* energy histogram and the results reweighted back afterwards. The Wang-Landau histogram method [10,11] can be seen as combined data collection and post-processing; when the simulation is complete, we have built up an estimate $\hat{g}(\epsilon)$ of the density of states (DOS). For some situations like first-order transitions and disordered media these methods have been very efficient.

During the simulation we can build up an estimate of the complete density $P_\beta(O)$, and clearly it would be beneficial to utilize this information. This insight is the key to *histogram methods*. In 1989 Ferrenberg and Swendsen [12] published a method to combine results obtained at different couplings. The method was highly efficient, and Ferrenberg-Swendsen reweighting has become an essential tool for MC practitioners. The use of raw data from several couplings allows for reweighting to a much broader range of couplings than ordinary single histogram methods.

In 1990 Alves, Berg, and Villanova (ABV) [13] developed a variation of the Ferrenberg-Swendsen (FS) multihistogram technique specifically targeted at calculating the density of states. To apply the FS method one must solve a set of nonlinear equations self-consistently; this can fail if the overlap between the various histograms is insufficient. This is not the case for the ABV method which can always be applied as long as every histogram has a finite overlap with at least one other histogram. We have developed a method to calculate the DOS which is a minor variation of ABV's original method.

The density of states is an elusive quantity and not very much used in statistical mechanics. In addition to presenting a method to calculate $g(\epsilon)$ we have therefore also briefly discussed statistical mechanics based on $g(\epsilon)$ in Sec. III and several applications in Sec. IV. Some of these applications are well-known results from traditional canonical thermodynamics; however, there are also properties which are more easily learned based on microcanonical thermodynamics.

The main focus of this paper is to determine the density of states from *canonical* Monte Carlo simulations. The density of states is the central quantity in *microcanonical* thermodynamics; hence, this naturally becomes an important formalism for further analysis of the DOS-based results. The study of microcanonical thermodynamics has seen increasing interest the latest years; see, e.g., Ref. [14] for a general introduction and Refs. [15–17] for some recent applications.

The rest of the paper is organized as follows: In Sec. II we present the algorithm to calculate the density of states. Section III is devoted to a short discussion of statistical mechanics based on $g(\epsilon)$. In the final section, Sec. IV, we use the algorithm to study several different phase transitions.

*Electronic address: hove@bccs.no

II. ESTIMATING $g(\epsilon)$

When doing a MC simulation with the Metropolis algorithm[1] the probability to be in a state ψ with energy ϵ_ψ is proportional to

$$g(\epsilon_\psi)e^{-\beta\epsilon_\psi}. \tag{3}$$

If we record a histogram of energies from a simulation at coupling β, we get a histogram $h_\beta(\epsilon)$ which is proportional to $g(\epsilon)e^{-\beta\epsilon}$. Multiplying this histogram by $e^{\beta\epsilon}$ we get something which is proportional to $g(\epsilon)$; i.e.,

$$\hat{g}_\beta(\epsilon) = e^{\xi_\beta}e^{\beta\epsilon}h_\beta(\epsilon) \tag{4}$$

is an estimator for $g(\epsilon)$. In Eq. (4), e^{ξ_β} is a dimensionless constant of proportionality to be determined. The density of states in Eq. (4) has an index β to indicate that the histogram was recorded at this coupling, but it does not have any intrinsic temperature dependence. In principle, Eq. (4) can be used to estimate $g(\epsilon)$ regardless of temperature; however, practically only a small energy range around $\langle E\rangle(T)$ will be sampled with a sufficiently high frequency.

Although Eq. (4) is useless as an immediate estimator for $g(\epsilon)$, it provides a basis for *combining* results from different couplings to an estimator $\hat{g}(\epsilon)$ which can be applied over the complete energy range. Given N different histograms $h_i(E)$ recorded at the couplings $\beta_1 > \beta_2 > \cdots > \beta_N$, we can combine them as

$$\hat{g}(\epsilon) = g_0\sum_{i=1}^{N} e^{\xi_i}h_i(\epsilon)w_i(\epsilon)e^{\beta_i\epsilon},$$

$$w_i(\epsilon) = \frac{h_i(\epsilon)}{\sum_{i=1}^{N} h_i(\epsilon)}, \tag{5}$$

to obtain an estimator which is usable over the complete ϵ range $[\min_\epsilon h_i(\epsilon), \max_\epsilon h(\epsilon)]$. In Eq. (5), $w_i(\epsilon)$ is a weight function, which denotes the weight ascribed to histogram i in the estimation of $g(\epsilon)$. The constants e^{ξ_i} are determined by joining the various histograms.

The algorithm we have applied to determine ξ_i is to set ξ_1 to an arbitrary value and then compute $\xi_{i>1}$ by minimizing

$$\chi^2 = \sum_{i=1}^{N-1}\sum_{j=i+1}^{N}\sum_{\epsilon} h_i(\epsilon)h_j(\epsilon) \times \underbrace{(\xi_i + \beta_i\epsilon + \ln h_i(\epsilon) - \xi_j - \beta_j\epsilon - \ln h_j(\epsilon))^2}_{\ln \hat{g}_{\beta_i}(\epsilon) - \ln \hat{g}_{\beta_j}(\epsilon)}. \tag{6}$$

As indicated in Eq. (6) the central principle is to minimize the pairwise difference between all the $\hat{g}(\epsilon)$ estimates, where the estimates $\hat{g}_{\beta_i}(\epsilon)$ are given according to Eq. (4). Minimizing χ^2 with respect to ξ_i gives $N-1$ linear equations which can be solved by, e.g., LU decomposition. The algorithm described by ABV uses a different weight $w_i(\epsilon)$ and the coefficients ξ_i are determined from a recursive procedure; ξ_{i+1} is given by ξ_i and a function of the overlap between histogram $h_i(\epsilon)$ and $h_{i+1}(\epsilon)$ (i and $i+1$ are not necessarily ordered according to coupling; see Ref. [13] for details). Apart from these differences this algorithm coincides with the one by ABV.

When the coefficients ξ_i have been determined we have all the coefficients $\xi_{i>1}$ expressed in terms of ξ_1. For discrete models with a finite ground-state degeneracy g_0 we can determine ξ_1 by requiring $g(\epsilon_0) = g_0$, or alternatively if the *total number of states* is known, this can be used to normalize $g(\epsilon)$. In Sec. IV we will consider both discrete models where the complete normalization can be achieved and continuous models where ξ_1 must be left undetermined.

Use of Eq. (5) to determine $g(\epsilon)$ is in principle quite straightforward, but in practice it is important to be careful to avoid numeric underflow or overflow in intermediate steps; in particular, the implementation must ensure that only $\ln g(\epsilon)$ is needed in actual computations.

III. STATISTICAL MECHANICS FROM $g(\epsilon)$

Knowledge of $g(\epsilon)$ is in principle equivalent to knowledge of the partition function $Z(\beta)$; hence, all the properties of a system are contained in $g(\epsilon)$. However, $g(\epsilon)$ does not have a very prominent role in modern statistical mechanics. We will therefore express some important results based on $g(\epsilon)$ in this section; examples and applications are given in Sec. IV. The definition of temperature in statistical mechanics [18] is given by

$$\beta = \frac{\partial \ln g(\epsilon)}{\partial\epsilon}. \tag{7}$$

From this we find that the fundamental requirement $C_V(T) \geqslant 0$ is equivalent to $\partial_\epsilon^2 \ln g(\epsilon) \leqslant 0$. The limiting value $\partial_\epsilon \ln g(\epsilon) = \mathcal{C}$ is the signature of a phase transition. A finite-ϵ range with $\partial_\epsilon \ln g(\epsilon) = \mathcal{C}$ means that the temperature is unchanged for this ϵ range—i.e., an indication of a first-order transition; actually, as we shall see in Sec. IV B, this is slightly more complicated. When the width of the of linear part of $\ln g(\epsilon)$ diminishes the first-order transition is weakened; until $\partial_\epsilon^2 \ln g(\epsilon) = 0$ in an isolated point only, this is the manifestation of a critical point. If we differentiate Eq. (7) with respect to T we find the function $C_V(\epsilon)$:

$$C_V(\epsilon) = \frac{\mathrm{d}\epsilon}{\mathrm{d}T} = \frac{-[\partial_\epsilon \ln g(\epsilon)]^2}{\partial_\epsilon^2 \ln g(\epsilon)}. \tag{8}$$

From Eq. (8) we see that the critical properties and, in particular, the critical exponent α must be related to how $\partial_\epsilon^2 \ln g(\epsilon)$ approaches zero. To infer α directly from the behavior of $g(\epsilon)$ close to ϵ_c is difficult, but if we make the size dependence of $g(\epsilon)$ explicit, we can use finite-size scaling [6,19,20]. At the (pseudo)critical point in a finite system, C_V scales as $L^{d+\alpha/\nu}$. The factor $[\partial_\epsilon \ln g(\epsilon)]^2$ in Eq. (8) is just equal to β_c^2; hence, the critical properties must come from the second derivative

[1] Software to go through the steps described in Secs. II and III can be downloaded as a C library from http://www.ift.uib.no/~hove/libdos/

$$|\partial_\epsilon^2 \ln g(\epsilon,L)|L^d \propto L^{-\alpha/\nu}. \quad (9)$$

In general $\partial_\epsilon \ln g(\epsilon,L)$ will also have finite-size effects; however, for this only the *deviation* from the thermodynamic value will show critical scaling.

For microcanonical systems the externally specified variable is ϵ, and not T, and critical scaling is governed by the difference $|\epsilon-\epsilon_c|$; see, e.g., Ref. [20]. Using this Hüller and Pleimling have calculated the order parameter exponent β from microcanonical data from the two- and three-dimensional Ising model [15].

When we have $g(\epsilon)$ we can easily calculate $F(T)$ and $P(\epsilon,T)$:

$$F(T) = -T \ln \sum_\epsilon g(\epsilon) e^{-\beta\epsilon}, \quad (10)$$

$$P(\epsilon,T) = \frac{g(\epsilon)e^{-\beta\epsilon}}{\Sigma_\epsilon g(\epsilon)e^{-\beta\epsilon}}. \quad (11)$$

From $P(\epsilon,T)$ we can easily calculate the internal energy and all moments thereof. If we in addition to ϵ sample other operators like the magnetization, we can use $P(\epsilon,T)$ to find thermal averages of arbitrary operators:

$$\langle O\rangle_T = \sum_\epsilon \langle O\rangle_\epsilon P(\epsilon,T). \quad (12)$$

In Eq. (12), $\langle O\rangle_\epsilon$ is the mean of $\hat{O}$ for a given value of ϵ.

IV. SOME APPLICATIONS

In this section we present various applications of the method presented in the preceding sections. In Sec. IV A the results are benchmarked against the two-dimensional (2D) Ising model, where $F(T)$ has been determined exactly *even for finite systems* [21]. In Sec. IV B we investigate the way phase transitions reveal themselves in $g(\epsilon)$. In Sec. IV C we calculate the finite-size corrections to the free energy in a cylindrical geometry. For conformally invariant systems [22] this is universal [23,24] and can be used to calculate the conformal charge. We have determined the conformal charge for the 2D Ising model and the 2D $Q=3$ Potts model. In Sec. IV D we discuss the problems related to models with a continuous energy distribution and show that method is useful also for these systems, although less so. Finally in Sec. IV E we have applied the method to a large data set obtained from a previous study of the full Ginzburg-Landau (GL) model.

A. Comparisons with exact results

Due to Onsager's exact solution [25] the 2D Ising model has been one of the most-used benchmarks in statistical physics. For a rectangular lattice with periodic boundary the model has been solved in closed form even for finite systems [21]; this constitutes a very convenient benchmark for our approach. We have performed simulations on a 32×32 system with periodic boundary conditions and verified that within statistical error both $F(T)$ and $C_V(T)$ agree with the exact values; see Figs. 1 and 2.

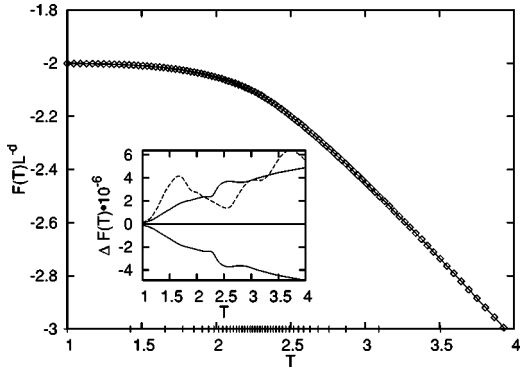

FIG. 1. Estimated value of $F(T)$ as symbols and the exact value from [21] as a solid line. The small ticks on the T axis indicate T values where simulations have been performed. In the inset the dashed curve shows the relative error of the estimated values, and the solid lines are $\pm$ an estimated statistical error.

The statistical errors indicated in Figs. 1 and 2 are calculated by performing ten completely independent simulations.

B. Signature of phase transitions in $g(\epsilon)$

As discussed in Sec. III all critical properties must be present in $g(\epsilon)$. In this section we will discuss the critical properties of the $Q=3$ and $Q=10$ Potts model. The first model has a continuous phase transition with $\alpha=1/3$ and $\nu=5/6$ [26]—i.e., $\alpha/\nu=0.4$—the second model has a first-order transition.

First we consider the $Q=3$ model; for this model, the goal is to determine the ratio α/ν from $g(\epsilon,L)$. According to Eq. (9) this can be done by considering how $\partial_\epsilon^2 \ln g(\epsilon,L)$ vanishes when approaching the critical energy ϵ_c. Figure 3 shows $L^d\partial_\epsilon^2 \ln g(\epsilon,L)$ for different system sizes, and we can see that the peak approaches zero with increasing system size.

In Fig. 4 we have plotted $\min|L^d\partial_\epsilon^2 \ln g(\epsilon,L)|$—i.e., the magnitude of the *peak* value for the curves in Fig. 3—as a function of L.

The dashed line in Fig. 4 has a slope of $-\alpha/\nu\approx-0.29$; this is a significant deviation from the exact value $\alpha/\nu=0.40$. However, we feel that these results are sufficient to

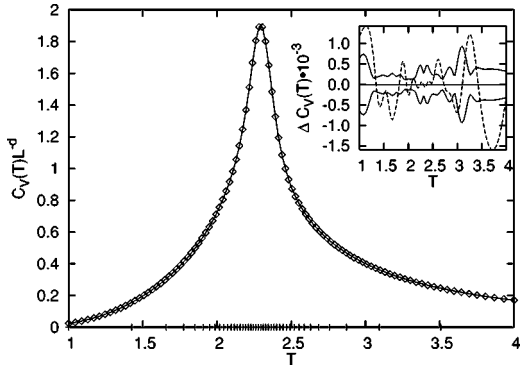

FIG. 2. Essentially the same as Fig. 1, but for the specific heat $C_V(T)$.

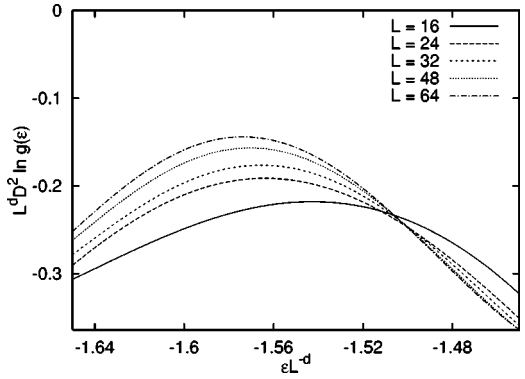

FIG. 3. $L^d \partial_\epsilon^2 \ln g(\epsilon, L)$ for different system sizes; in the limit $L \to \infty$ this vanishes as $L^{-\alpha/\nu}$.

demonstrate that the critical properties and, in particular, the exponents α and ν are contained in $g(\epsilon)$. There are clearly significant finite-size effects in $\partial_\epsilon \ln g(\epsilon, L)$ also; including the factor $\partial_\epsilon \ln g(\epsilon)$ gives the "improved" value $\alpha/\nu \approx 0.35$. However, this cannot contribute in the $L \to \infty$ limit and we have therefore not included this factor in Fig. 4. Finally Fig. 4 is based on the second derivative of a sampled quantity; hence, it will clearly be difficult to determine with high precision. In conclusion it is definitely *possible* to infer the ratio α/ν from the properties of $g(\epsilon, L)$, but it is certainly not the most suitable way for high-precision measurements. Finally we mention that the remaining critical exponents *cannot* be obtained from $g(\epsilon)$, their value is based on the explicit choice of fields to represent the critical state.

Although all thermodynamic information about a phase transition is contained in $F(T)$, it is only for a first-order transition, where $\partial_T F(T)$ is discontinous at T_c, that the phase transition stands out in $F(T)$. Figure 5 shows $F(T)$ for the strong transition in the two-dimensional $Q=10$ Potts model; a discontinuity in $\partial_T F(T)$ at $T \approx 0.71$ is easily spotted.

For second-order transitions we had to revert to FSS to infer critical properties from $g(\epsilon)$; in the case of first-order transitions, we can make quite powerful statements from $g(\epsilon)$ alone. Given a first-order transition between the pure states ϵ_1 and ϵ_2 the probability $P(\epsilon, T)$ is bimodal, with distinct peaks at the pure energy levels ϵ_1 and ϵ_2. The mixed states with energy $\epsilon_1 < \epsilon < \epsilon_2$ are exponentially suppressed; to reproduce this behavior, we must have

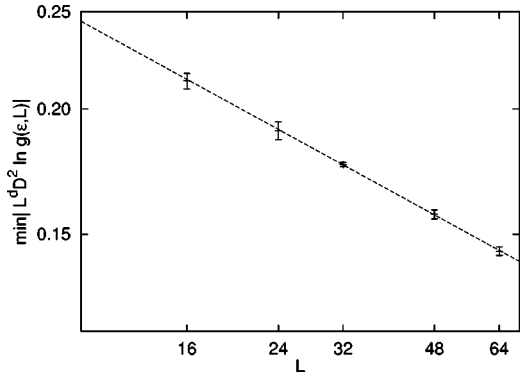

FIG. 4. Finite-size scaling of $L^d \min|\partial_\epsilon^2 g(\epsilon, L)|$ in a log-log plot; the dashed line has a slope $-\alpha/\nu \approx -0.29$.

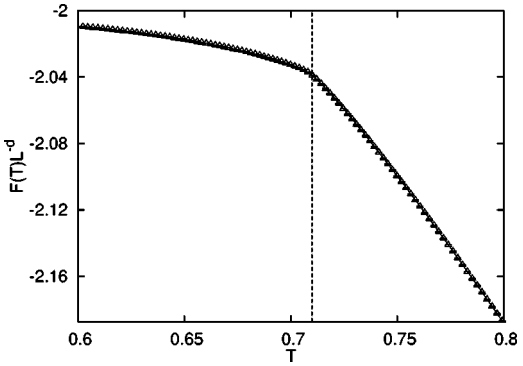

FIG. 5. The free energy $F(T)$ for the $Q=10$ Potts model which has a strong first-order transition. Although there is inevitably some finite-size rounding, the cusp in this figure is quite clear. Figure 1 shows a similar figure for a continuous transition; this is clearly smooth in comparison.

$$\ln g(\epsilon_1 + \Delta\epsilon) < \ln g(\epsilon_1) + \beta \ln\left(\frac{g(\epsilon + \Delta\epsilon)}{g(\epsilon)}\right) \qquad (13)$$

for $0 < \Delta\epsilon < \epsilon_2 - \epsilon_1$. Hence $\ln g(\epsilon)$ must increase *weaker* than linearly in the immediate vicinity of ϵ_1 and then subsequently stronger than linearly afterwards such that the relation $\beta_c = \partial_\epsilon \ln g(\epsilon_1) = \partial_\epsilon g(\epsilon_2)$ is satisfied. If we insist on $\partial_\epsilon^2 \ln g(\epsilon) \leqslant 0$ also in the interval $\epsilon_1 < \epsilon < \epsilon_2$, $\ln g(\epsilon)$ must have a *cusp* in this interval; however, these energy levels correspond to states which are manifest not equilibrium, so it might be too strict to require $\partial_\epsilon^2 \ln g(\epsilon) \leqslant 0$ in this particular interval. An extensive discussion of the region $\epsilon_1 < \epsilon < \epsilon_2$ can be found in Ref. [27]. The various details of $g(\epsilon)$ around a first-order transition are illustrated in Fig. 6.

C. Conformal charge

It is well known that critical systems are *scale invariant*; in addition, the critical systems often possess further symmetries like translational and rotational invariance. Together these operations form a group $\mathcal{G}$. Under quite mild restrictions, in particular finite-length interactions, the system is actually invariant also under transformations which *vary in space*; this means that $\mathcal{G}$ is the conformal group. In particular for $d=2$ this is a very powerful result, and the application of conformal field theory (CFT) has led to many exact results for the critical state [28].

Consider an infinitely long strip of width W. Due to the finite width, there will be finite-size corrections to the free energy density. One of the most fundamental results from conformal invariance is that the leading finite-size correction for this system is universal [23,24]:

$$f_W = f_B - \frac{\pi c}{6W^2} + \mathcal{O}\left(\frac{1}{W^4}\right). \qquad (14)$$

In Eq. (14), f_W is the free energy density of the strip, f_B is the bulk free energy density of an infinite system, and c is the conformal charge or anomaly. The conformal charge is a dimensionless number which uniquely characterizes a given universality class. In two dimensions the Ising model has c

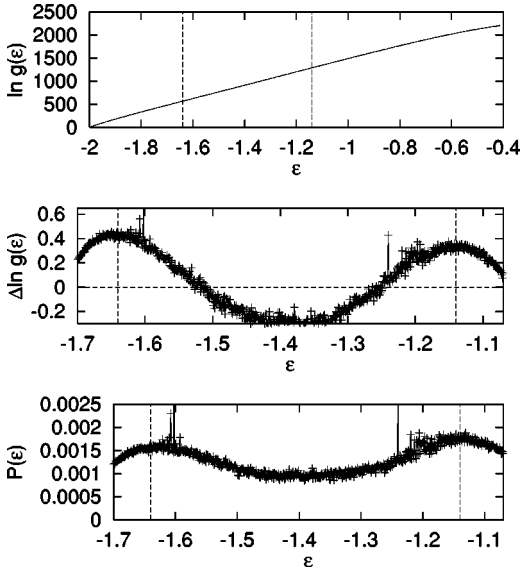

FIG. 6. Results from the $Q=10$ Potts model. The uppermost panel shows $\ln g(\epsilon)$; the two dashed lines indicate the two energy levels ϵ_1 and ϵ_2. The central panel shows $\ln g(\epsilon)-[\beta(\epsilon-\epsilon_1)+\ln g(\epsilon_1)]$, which clearly shows that $\ln g(\epsilon)$ has small but significant deviations from perfect linearity in the range $\epsilon_1<\epsilon<\epsilon_2$. The bottom panel shows $P(\epsilon,T_c)$—i.e., Eq. (11) at the critical point—and we can clearly see how the depression in $P(\epsilon,T_c)$ originates from the features in $\ln g(\epsilon)$. This figure very closely resembles Fig. 1 of Ref. [27].

$=0.5$ and the $Q=3$ Potts model has $c=0.8$ [22].

Equation (14) is a finite-size scaling expression which should be very useful for numeric evaluation of c. However, since the use of Eq. (14) requires knowledge of the free energy, MC simulations have not been extensively used; see, however, for instance, [29] for a numerical test of another conformal field theory conjecture by MC methods. The numerical evaluation of c has been dominated by transfer matrix methods [22,30]; see, however, Ref. [31] for a study of the $Q=3$ Potts model very similar to the present one.

Using the method presented in this paper we have calculated c for the Ising model and the $Q=3$ Potts model. We have considered cylindrical systems of length L and circumference W, we have considered $W=\{4,5,6,8,10,12,16\}$, and for each W we have used $L=\{W,2W,4W,8W,(16W)\}$; $L=16W$ was only considered for the Ising model. From this we have extrapolated to find

$$f_W=\lim_{L\to\infty}\frac{1}{LW}F(L,W). \tag{15}$$

Plots of f_W are shown in Fig. 7, and c has been determined from a least-squares fit to these curves. The curves in Fig. 7 show that there are quite significant corrections to the W^{-2} term for small W, and the numerical results $c=0.49\pm0.07$ for the Ising model were obtained by excluding all $W<8$. Including an additional fourth-order term [30] and including all the results, we get $c=0.55\pm0.06$. Most of the computational resources were spent on the Ising model, and the $Q=3$ Potts results are lower quality. The solid line corresponds to $c=0.86\pm0.19$; this was obtained by retaining only the four largest W values.

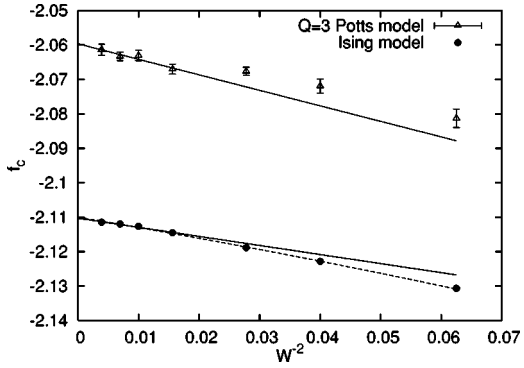

FIG. 7. The extrapolated limit f_W from Eq. (15) for the Ising and $Q=3$ Potts model. The conformal charge is given by the slope in the $W^{-2}\to 0$ limit. The solid line is a least-squares fit to Eq. (14) and the dashed line comes from including an additional term αW^{-4} in the fit. For the Ising model the error bars are smaller than the symbol size.

D. Continuous systems

The method we have presented can to some extent also be applied to systems with a continuous energy distribution; however, for these systems the full normalization of $g(\epsilon)$ is difficult. The method used to normalize $g(\epsilon)$ for discrete systems so far requires that (i) the ground state be sampled and (ii) that the histograms have sufficient overlap. For a system with a truly continuous energy distribution sampling of the ground state requires $T\equiv 0$, and this will generate histograms without overlap. Even for models with a very small energy gap, like, e.g., the Z_q [32] model for large q, a large fraction of the computational resources must be spent close to the ground state to ensure that both conditions are met. Attempts to generalize the Wang-Landau histogram sampling to continuous systems are faced with essentially the same problems [33].

Due to problems with the normalization, we must generally be content with a function $\ln\tilde{g}(\epsilon)=\ln g(\epsilon)+\mathcal{C}$ where $\mathcal{C}$ is an unknown, dimensionless constant. This will induce a linear error $\Delta F(T)=-T\ln\mathcal{C}$ in the free energy, but since Eq. (11) is independent of $\mathcal{C}$, all remaining thermodynamics will be unaffected by the incomplete normalization.

The Z_q clock model is a planar spin model where the real angle $\phi\in[0,2\pi\rangle$ is approximated with the discrete variable $\theta_i=i2\pi/q$; in the limit $q\to\infty$, this converges to the XY model. Numerical simulations of the XY model are customarily done using the Z_q model with q "large enough"; values of $q=32$ or 64 are often used. Furthermore, it has been shown that already at $q=5$ the critical properties are governed by the XY critical point [32,34]. To learn about the behavior $g(\epsilon)$ for continuous systems we have done a short simulation of a 32×32 system for the Z_q model with $q=2048$; according to the discussion above, this should capture the properties of the continuous $q\to\infty$ system. Figure 8 shows $\ln g(\epsilon)$ for the Z_q model with $q=2048$ along with the Ising model.

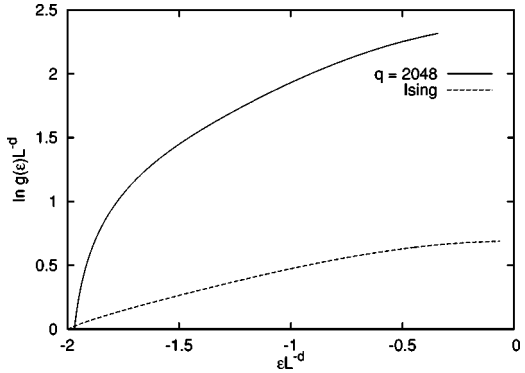

FIG. 8. Comparison of $\ln g(\epsilon)$ for the $q=2048$ Z_q model and the Ising model. Observe that the curve for the Z_q model has been vertically shifted by an *unknown* amount; see text.

For the Z_q model the lowest lying of the sampled states has energy ϵ_-; hence, the Z_q curve in Fig. 8 terminates at this ϵ value. This means that $g(\epsilon)$ is undetermined in the interval $[\epsilon_0, \epsilon_-\rangle$, where $\epsilon_0=-2L^d$ is the ground-state energy. Furthermore, overall normalization is impossible to determine, and we have just arbitrarily fixed $\ln g(\epsilon_-)=0$.

According to Eq. (11) the internal energy and specific heat depend only on the shape of $\ln g(\epsilon)$, and not the possible vertical offset. Combined with the knowledge from previous simulations—that the Z_q model for large q correctly captures the thermodynamics of the *XY* model—we can conclude that apart from the vertical offset, Fig. 8 is a faithful representation of $g(\epsilon)$ for the continuous *XY* model. Looking at Fig. 8 the most striking features are (i) $g(\epsilon)$ is orders of magnitude larger for the Z_q model than the Ising model and (ii) the steep sloop of $\ln g(\epsilon)$ for the Z_q model; actually, any gapless model must have $\lim_{\epsilon\to\epsilon_0}\partial_\epsilon g(\epsilon)\to\infty$ to produce a finite value for $C_V(T)$ in the limit $T\to 0$.

In Sec. IV E we will reanalyze a real data set from large scale simulations of the Ginzburg-Landau model; this constitutes a real example of a continuous system.

E. Reanalyzing Ginzburg-Landau results

The GL model is one of the most studied models in physics, and it is applied as a "meta model" in a wide range of fields; see Ref. [35] for an extensive list of applications. In dimensionless form, the continuum version of the model is given by the functional integral

$$Z=\int \mathcal{D}A_\nu \mathcal{D}\phi \exp\left[-\int d^dr\left[\frac{1}{4}F_{\mu\nu}^2+|(\partial_\nu+iA_\nu)\phi|^2 + y|\phi|^2+x|\phi|^4\right]\right]. \quad (16)$$

In Eq. (16), ϕ is a complex condensate field, **A** is the electromagnetic gauge field, and x and y are parameters. The system is driven through a phase transition by the temperaturelike parameter y, and the qualitative behavior at the phase transition is governed by x. For large x amplitude fluctuations in ϕ are suppressed, leaving only *phase fluctuations*,

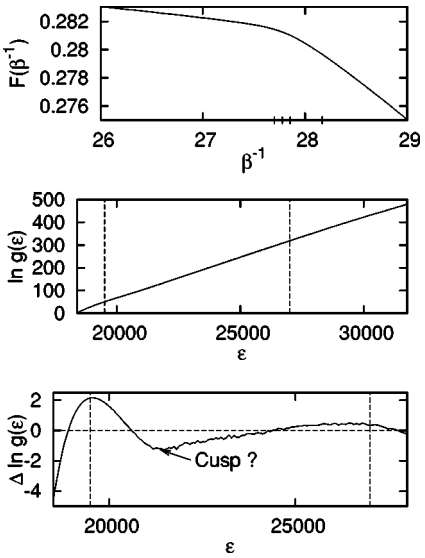

FIG. 9. The upper part shows the free energy $F(\beta)$; although it is rounded, we can clearly see the remnants of a cusp in $F(\beta)$. The thin ticks on the x axis indicate the couplings which where used. The central figure shows $\ln g(\epsilon)$; the dashed lines indicate the two metastable energy levels ϵ_1 and ϵ_2. In the lowest figure we have plotted $\ln g(\epsilon)-\hat{g}(\epsilon)$, where $\hat{g}(\epsilon)$ is a fit to a straight line on the interval $\epsilon_1<\epsilon_2$. Although not very prominent, the structure in this plot is significant; see the discussion at the end of Sec. IV B. The results come from a simulation of a system of $40\times40\times40$ lattice units.

and the transition is second order. In the limit $x\to 0$ the amplitude fluctuations dominate, and the transition is first order. For intermediate values of x all the degrees of freedom influence the dynamics, and for $x=x_T$ the transition changes order at a tricritical point [35].

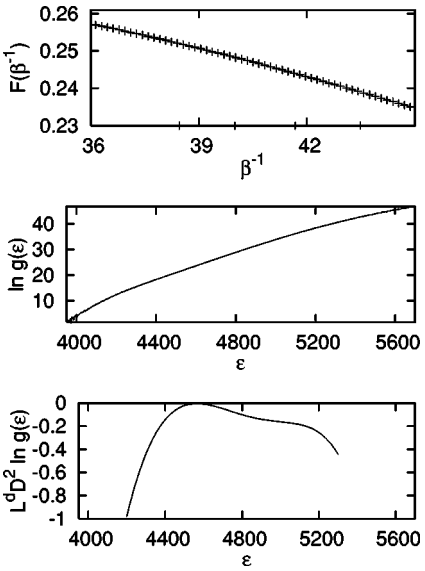

FIG. 10. The two upper panels show the same as Fig. 9, for a second-order transition. The lower panel shows $\partial_\epsilon^2 \ln g(\epsilon)$, and we can see that this approaches zero at the critical energy $\epsilon_c\approx 4600$; this can be compared to Fig. 3.

In 2001 we determined the tricritical value x_T from large-scale Monte Carlo simulations [35]. Here we have reanalyzed some of the data from this simulation. Figure 9 shows results for the GL model for $x < x_T$—i.e., a first-order transition. The upper panel of this figure can be compared with Fig. 5, and the two *lower* panels can be compared with the two *upper* panels of Fig. 6.

Figure 10 is similar to Fig. 9, but for $x > x_T$—i.e., a second-order transition.

Due to the difficulties mentioned in Sec. IV D, we are not able to calculate the overall normalization g_0 of $g(\epsilon)$. Nevertheless, $g(\epsilon)$ shows the critical behavior discussed in Sec. IV B, and the behavior of $F(y)$ clearly separates between first- and second-order transitions.

In conclusion we feel that in applications to the GL model the method has proved itself, and furthermore that it provides interesting information even though g_0 cannot be determined.

ACKNOWLEDGMENTS

The author gratefully acknowledges comments on an early version of the manuscript from Alexander Hartmann. A discussion with Kari Rummukainen is also acknowledged.

[1] N. Metropolis, A. W. Rosenbluth, M. N. Rosenbluth, A. H. Teller, and E. Teller, J. Chem. Phys. **21**, 1087 (1953).
[2] Barry A. Cipra, SIAM News **33**(4) (2000).
[3] J. E. Gubernatis, *The Monte Carlo Method in the Physical Sciences: Celebrating the 50th Anniversary of the Metropolis Algorithm* (AIP, Melville, NY, 2003).
[4] D. P. Landau and K. Binder, *A Guide to Monte Carlo Simulations in Statistical Physics* (Cambridge University Press, Cambridge, England, 2000).
[5] K. P. N. Murthy, *Monte Carlo Methods in Statistical Physics* (Universities Press, India, 2004).
[6] K. Binder and D. W. Heermann, *Monte Carlo Simulations in Statistical Physics* (Springer-Verlag, Berlin, 1997).
[7] B. A. Berg, e-print cond-mat/9909236.
[8] B. A. Berg and T. Neuhaus, Phys. Rev. Lett. **68**, 9 (1992).
[9] B. A. Berg, Comput. Phys. Commun. **153**, 397 (2003).
[10] F. Wang and D. P. Landau, Phys. Rev. Lett. **86**, 2050 (2001).
[11] F. Wang and D. P. Landau, Phys. Rev. E **64**, 056101 (2001).
[12] A. M. Ferrenberg and R. H. Swendsen, Phys. Rev. Lett. **63**, 1195 (1989).
[13] N. A. Alves, B. A. Berg, and R. Villanova, Phys. Rev. B **41**, 383 (1990).
[14] D. H. E. Gross, *Microcanonical Thermodynamics: Phase Transitions in "Small" Systems* (World Scientific, Singapore, 2001).
[15] A. Hüller and M. Pleimling, Int. J. Mod. Phys. C **13**, 947 (2002).
[16] H. Behringer, J. Phys. A **36**, 8739 (2003).
[17] H. Behringer, J. Phys. A **37**, 1443 (2004).
[18] F. Reif, *Fundamentals of Statistical and Thermal Physics* (McGraw-Hill, New York, 1985).
[19] M. Kastner, M. Promberger, and A. Hüller, J. Stat. Phys. **99**, 1251 (2000).
[20] M. Kastner and M. Promberger, J. Stat. Phys. **103**, 893 (2001).
[21] A. E. Ferdinand and M. E. Fisher, Phys. Rev. **185**, 185 (1969).
[22] M. Henkel, *Conformal Invariance and Critical Phenomena* (Springer-Verlag, Berlin, 1999).
[23] H. W. J. Blöte, J. L. Cardy, and M. P. Nightingale, Phys. Rev. Lett. **56**, 742 (1986).
[24] I. Affleck, Phys. Rev. Lett. **56**, 746 (1986).
[25] L. Onsager, Phys. Rev. **65**, 117 (1944).
[26] D. A. Lavis and G. M. Bell, *Statistical Mechanics of Lattice Systems 2* (Springer-Verlag, Berlin, 1999).
[27] D. H. E. Gross, e-print cond-mat/0307054.
[28] J. Cardy, *Scaling and Renormalization in Statistical Physics* (Cambridge University Press, Cambridge, England, 1997).
[29] M. Weigel and W. Janke, Europhys. Lett. **51**, 578 (2000).
[30] V. Dotsenko, J. L. Jacobsen, M.-A. Lewis, and M. Picco, Nucl. Phys. B **546**, 505 (1999).
[31] G. Ódor, Int. J. Mod. Phys. C **3**, 1195 (1992).
[32] S. Elitzur, R. B. Pearson, and J. Shigemitsu, Phys. Rev. D **19**, 3698 (1979).
[33] Thomad Ramstad, Master thesis, NTNU, 2003 (http://www.phys.ntnu.no/~thomaram/thesis).
[34] J. Hove and A. Sudbø, Phys. Rev. E **68**, 046107 (2003).
[35] S. Mo, J. Hove, and A. Sudbø, Phys. Rev. B **65**, 104501 (2002).